Journal of Systems Engineering and Electronics
Vol. 31, No. 4, August 2020, pp.791 – 803

Multiconstraint adaptive three-dimensional guidance law using convex optimization

FU Shengnan[1], LIU Xiaodong[2], ZHANG Wenjie[3], and XIA Qunli[3,*]

1. School of Mechatronical Engineering, Beijing Institute of Technology, Beijing 100081, China;
2. Beijing Aerospace Automatic Control Institute, Beijing 100854, China;
3. School of Aerospace Engineering, Beijing Institute of Technology, Beijing 100081, China

Abstract: The traditional guidance law only guarantees the accuracy of attacking a target. However, the look angle and acceleration constraints are indispensable in applications. A new adaptive three-dimensional proportional navigation (PN) guidance law is proposed based on convex optimization. Decomposition of the three-dimensional space is carried out to establish three-dimensional kinematic engagements. The constraints and the performance index are disposed by using the convex optimization method. PN guidance gains can be obtained by solving the optimization problem. This solution is more rapid and programmatic than the traditional method and provides a foundation for future online guidance methods, which is of great value for engineering applications.

Keywords: proportional navigation (PN), adaptive guidance law, three-dimensional space, second-order cone programming (SOCP), convex optimal control.

DOI: 10.23919/JSEE.2020.000054

1. Introduction

In recent years, convex optimization has been applied to aerospace problems, such as planetary landing [1 – 5], spacecraft rendezvous and proximity operations [6 – 8], and spacecraft trajectory planning [9 – 12]. Second-order cone programming (SOCP) is the most commonly used method in convex optimization [13,14], and it can obtain a feasible solution without accurate initialization [15]. If there is no feasible solution, then this method can conclude that the problem is unsolvable.

Research on the association of the guidance law and convex optimization, especially the proportional navigation (PN) guidance law [16 – 18], is attracting the attention of many researchers. The PN guidance law requires limited information [19,20] to attack a stationary target. However, for an expected impact path angle, the terminal constraint cannot be satisfied with a constant guidance gain.

Previous work includes two main classes of approaches to satisfy the impact angle constraint. (i) Based on the pure proportional navigation (PPN) guidance law, a biased pure proportional navigation (BPPN) guidance law [21] shapes the trajectory using a bias term. The term is integrated continuously before reaching a certain threshold and transforms the BPPN guidance law into the PPN guidance law. This law is an open-loop guidance law, with imprecision occurring if interrupted. Song and Zhang [22] designed a variable structure PN guidance law to realize the constraint of the terminal attack angle by estimating the distance between a missile and a target as well as the rate of the distance. (ii) Zhang et al. [23] designed a sliding mode controller that satisfies the constraint of the terminal attack angle by executing the sliding mode. The sliding mode function and its derivative converge to 0 near the sliding surface by backstepping. The controller can deal with the lag of high-order systems with good robustness. A new integrated guidance and control design scheme based on the variable structure control approach [24] is established to hit the target with both the desired impact angle and the desired flight attitude angle. Shashi et al. [25] proposed a guidance strategy that caters to both the impact angle and the impact time terminal constraints.

In addition to the impact path angle constraint, the look angle constraints should also be considered due to the seeker's field-of-view constraint. Park et al. [26] proposed a multistage guidance law for stationary targets. The flight stage is divided into three stages: (i) the initial phase, where the look angle is controlled to reach the maximum; (ii) the middle phase, where the maximum look angle is maintained; and (iii) the terminal phase, where the impact angle is constrained to attack the target. Tekin and Erer

Manuscript received August 01, 2019.
*Corresponding author.
This work was supported by the National Natural Science Foundation of China (61803357).

[27] designed unbiased and biased compound proportional guidance laws using a switch strategy for the guidance gain to ensure different constraints; then, other modified PN guidance laws with a time-varying bias term [28,29] reduced the look angle monotonically to 0.

For engineering applications, acceleration is subject to maneuverability and physical structure. Liu et al. [30] proposed a time-varying PN guidance law based on convex optimization. The solution time is significantly shortened compared with that of the traditional optimization method. Huan et al. [31] improved the time-varying PN guidance law for cooperative guidance to realize the simultaneous attack of multiple missiles.

This paper presents a further study on the basis of [30]. We develop a three-dimensional kinematic engagement model subject to multiple constraints based on convex optimization

The remainder of this paper is organized as follows. A three-dimensional kinematic engagement model and the equation of state are established in Section 2. All constraints are introduced, and the optimal convex control problem is established in Section 3. A successive process is formulated to solve the control problem in Section 4. The verification of the simulation model is presented, and the numerical results are discussed in Section 5. The most important conclusions are summarized in Section 6.

2. Problem formulation

2.1 Three-dimensional decomposition

The relationship between a missile M and a stationary target T in three-dimensional space is established in Fig. 1.

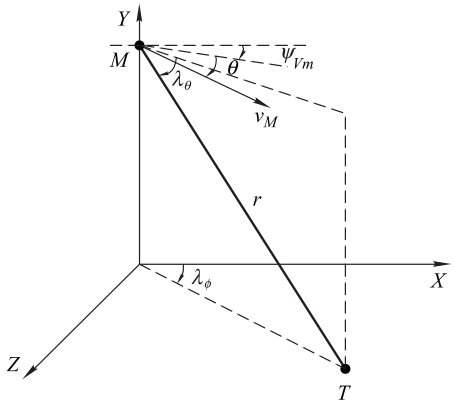

Fig. 1 Standard three-dimensional relative motion relationship

r is the range between the missile and the target, v_M is the missile's velocity, θ is the flight path angle, ψ_{Vm} is the heading angle, λ_θ is the line-of-sight (LOS) angle of the pitch channel, and λ_ϕ is the LOS angle of the yaw channel.

Because a standard three-dimensional engagement cannot be convex, the three-dimensional relationship is decomposed into a vertical plane MVT and a lateral plane MLT in Fig. 2 based on the assumption that the mutual coupling between the planes can be ignored. The subscripts V and L indicate variables in planes MVT and MLT, respectively.

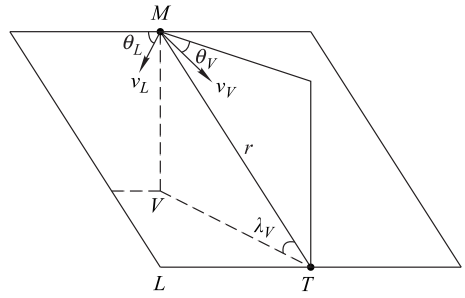

Fig. 2 Three-dimensional relative motion relationship

The velocity of the missile v_M is decomposed into v_V and v_L for the planes:

$$v_V = \sqrt{v_x^2 + v_y^2}, \tag{1}$$

$$v_L = \sqrt{v_x^2 + v_z^2}, \tag{2}$$

where

$$v_x = v_M \cos\theta \cos(\psi_{Vm} - \lambda_\phi) \cos\lambda_\theta + v_M \sin\theta \sin\lambda_\theta,$$

$$v_y = v_M \cos\theta \cos(\psi_{Vm} - \lambda_\phi) \sin\lambda_\theta + v_M \sin\theta \cos\lambda_\theta,$$

$$v_z = v_M \cos\theta \sin(\psi_{Vm} - \lambda_\phi).$$

To more accurately model the two-dimensional plane, we design relationships between a missile and a stationary target for different planes in Fig. 3 where v is the missile's velocity, a is the lateral acceleration perpendicular to the velocity, λ is the LOS angle, and ε is the look angle.

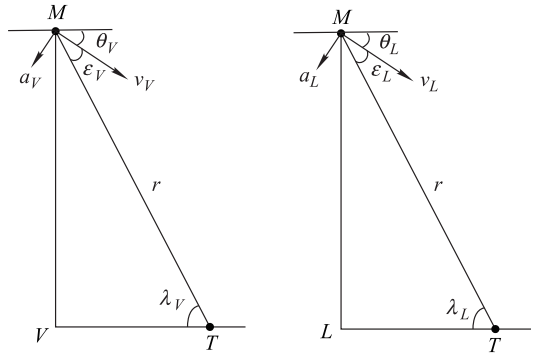

(a) Vertical plane (b) Lateral plane

Fig. 3 Relative motion relationship for different planes

Angles between the two-dimensional planes and the three-dimensional space need to be correlated. Plane MCD in Fig. 4 corresponds to plane MVT, and plane MBC is designed as the horizontal plane. Line MB is the projection of the velocity v_M on the horizontal plane, and

line MC is the projection of MB on plane MCD. The relationship between the decomposed three-dimensional plane in Fig. 2 and the standard three-dimensional space in Fig. 4 is established by the projection.

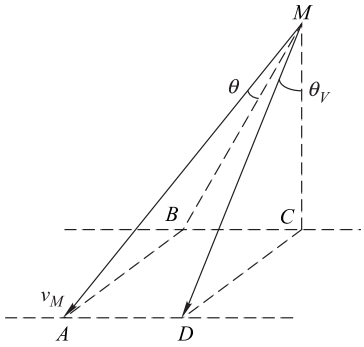

Fig. 4 Projection relationship

Based on Fig. 4, numerical relations can be derived: $\angle AMB = \theta$, $\angle BMC = \psi_{Vm} - \lambda_\phi$, $\angle ADM = 90°$, $\angle ABM = 90°$, $\angle BCM = 90°$, $\angle DCM = 90°$.

We can obtain $AB \perp MBC$ and $DC \perp MBC$ from the above relationships. Then, we have $AB // DC$. $AD // BC$ is derived using the same method. In other words, the parallelogram $ABCD$ yields $AB = DC$. The angle relationship is given as follows:

$$\tan\theta_V = \frac{DC}{MC} = \frac{v_M \sin\theta}{v_M \cos\theta \cos(\psi_{Vm} - \lambda_\phi)} = \frac{\tan\theta}{\cos(\psi_{Vm} - \lambda_\phi)}. \tag{3}$$

When considering only the guidance of the vertical plane MVT, the assumption $\psi_{Vm} \approx \lambda_\phi$ is made. Similarly, for the lateral plane MLT, we suppose $\theta \approx \lambda_\theta$.

The angle relationships between the decomposed three-dimensional space and the three-dimensional space can be obtained:

$$\theta_V \approx \theta, \tag{4}$$

$$\theta_L \approx \psi_{Vm}. \tag{5}$$

2.2 Two-dimensional engagement kinematics with PN

Once the three-dimensional space has been decomposed, the guidance law can be designed separately for the planes to realize three-dimensional guidance that ignores the mutual coupling between planes. For example, for plane MVT, two-dimensional engagement kinematics with the PN guidance law can be described as follows:

$$\frac{\mathrm{d}r}{\mathrm{d}t} = -v_V \cos\varepsilon_V, \tag{6}$$

$$r\frac{\mathrm{d}\lambda_V}{\mathrm{d}t} = -v_V \sin\varepsilon_V, \tag{7}$$

$$r\frac{\mathrm{d}\varepsilon_V}{\mathrm{d}t} = -(N_V - 1)v_V \sin\varepsilon_V \tag{8}$$

where N_V is the guidance coefficient.

The engagement kinematics for plane MLT can be derived using the same approach. To facilitate subsequent linearization, the independent variable of the two-dimensional kinematics is changed from t to r, namely, (7) and (8) are divided by (6), which produces the following:

$$r\lambda_V' = \sigma_V, \tag{9}$$

$$r\varepsilon_V' = (N_V - 1)\sigma_V, \tag{10}$$

where $\sigma_V = \tan\varepsilon_V$ to realize the linearization and the independent variable r is hidden for simplicity. The lateral acceleration command is given as follows:

$$a_{Vc} = v_V \frac{\mathrm{d}\theta_V}{\mathrm{d}t} = N_V v_V \frac{\mathrm{d}\lambda_V}{\mathrm{d}t} = -\frac{N_V v_V^2 \sin\varepsilon_V}{r}. \tag{11}$$

The following assumptions are made:

(i) The dynamics of the control system can be neglected, and $a_V = a_{Vc}$, where a_{Vc} denotes the acceleration command and a_V denotes the actual acceleration.

(ii) The autopilot missile is significantly faster than the guidance loop.

2.3 Three-dimensional equation of states and linearization

The engagement kinematics of plane MVT and plane MLT are merged, and the result is rewritten as an equation of the state:

$$r\boldsymbol{x}' = \boldsymbol{f}(\boldsymbol{x}) + \boldsymbol{B}(\boldsymbol{x})\boldsymbol{u} \tag{12}$$

where $\boldsymbol{x} = (\lambda_V \quad \sigma_V \quad \lambda_L \quad \sigma_L)^{\mathrm{T}}$ is the state vector, $\boldsymbol{u} = (N_V \quad N_L)^{\mathrm{T}}$ is the control vector, and

$$\boldsymbol{f}(\boldsymbol{x}) = \begin{pmatrix} \sigma_V \\ -\sigma_V(1+\sigma_V^2) \\ \sigma_L \\ -\sigma_L(1+\sigma_L^2) \end{pmatrix},$$

$$\boldsymbol{B}(\boldsymbol{x}) = \begin{pmatrix} 0 & 0 \\ \sigma_V(1+\sigma_V^2) & 0 \\ 0 & 0 \\ 0 & \sigma_L(1+\sigma_L^2) \end{pmatrix}.$$

In the three-dimensional equation of the state, control vectors are decoupled from state vectors to achieve the convergence of optimization using sequential programming methods. For application to the convex optimization method, the equation of the state needs to be partially linearized. Let $\{\boldsymbol{x}^{(k)}, \boldsymbol{u}^{(k)}\}$ be the kth successive solution. $\boldsymbol{f}(\boldsymbol{x})$ is linearized at $\boldsymbol{x}^{(k)}$, and $\boldsymbol{B}(\boldsymbol{x})$ is approximated by $\boldsymbol{B}(\boldsymbol{x}^{(k)})$, thus yielding

$$r\boldsymbol{x}' = \boldsymbol{A}(\boldsymbol{x}^{(k)})\boldsymbol{x} + \boldsymbol{B}(\boldsymbol{x}^{(k)})\boldsymbol{u} + \boldsymbol{c}(\boldsymbol{x}^{(k)}) \tag{13}$$

where $\boldsymbol{x}^{(k)} = (\lambda_V^{(k)} \quad \sigma_V^{(k)} \quad \lambda_L^{(k)} \quad \sigma_L^{(k)})^{\mathrm{T}}$ and

$$\boldsymbol{A}(\boldsymbol{x}^{(k)}) = \frac{\partial \boldsymbol{f}(\boldsymbol{x}^{(k)})}{\partial \boldsymbol{x}} = \begin{pmatrix} 0 & 1 & 0 & 0 \\ 0 & -1-3(\sigma_V^{(k)})^2 & 0 & 0 \\ 0 & 0 & 0 & 1 \\ 0 & 0 & 0 & -1-3(\sigma_L^{(k)})^2 \end{pmatrix},$$

$$\boldsymbol{B}(\boldsymbol{x}^{(k)}) = \begin{pmatrix} 0 & 0 \\ \sigma_V^{(k)} + (\sigma_V^{(k)})^{(3)} & 0 \\ 0 & 0 \\ 0 & \sigma_L^{(k)} + (\sigma_L^{(k)})^{(3)} \end{pmatrix},$$

$$\boldsymbol{c}(\boldsymbol{x}^{(k)}) = \boldsymbol{f}(\boldsymbol{x}^{(k)}) - \boldsymbol{A}(\boldsymbol{x}^{(k)})\boldsymbol{x}^{(k)} = \begin{pmatrix} 0 \\ 2(\sigma_V^{(k)})^3 \\ 0 \\ 2(\sigma_L^{(k)})^3 \end{pmatrix}.$$

To validate the linearization, a trust-region constraint is chosen as follows:

$$|\boldsymbol{x} - \boldsymbol{x}^{(k)}| \leqslant \boldsymbol{\delta} \tag{14}$$

where $\boldsymbol{\delta} \in \mathbf{R}^2$ is a constant vector. This constraint needs to be relaxed to increase the efficiency during optimization.

3. Optimal control problem

3.1 Objective function

For optimization problems, appropriate optimization objectives are necessary to realize different performance indexes. Common optimization objectives include the maximum range, the minimum range, and the minimum time. The objective in this paper is to minimize the control energy, which corresponds to the following objective function:

$$J = \frac{-\displaystyle\int_{r_0}^{r_f} (v_V^3 \sigma_V \sin\varepsilon_V N_V^2 + v_L^3 \sigma_L \sin\varepsilon_L N_L^2)\mathrm{d}r}{r^2} \tag{15}$$

where r_0 is the initial range between the missile and the target, r_f is the terminal range between the missile and the target, $\varepsilon_V = \arctan\sigma_V$ and $\varepsilon_L = \arctan\sigma_L$.

3.2 Constraints

Once a scenario is designed, the mission has requirements in terms of initial states and terminal states. Considering the physical constraints, the guidance law is subject to the field of view and the acceleration. To achieve convexity, these constraints are denoted as a linear form or a second-order cone form.

(i) Initial constraints:

$$\begin{cases} r_0 = r(r_0) \\ \lambda_{V_0} = \lambda_V(r_0) \\ \varepsilon_{V_0} = \varepsilon_V(r_0) \\ \lambda_{L_0} = \lambda_L(r_0) \\ \varepsilon_{L_0} = \varepsilon_L(r_0) \end{cases}. \tag{16}$$

(ii) Look angle constraints:

$$\begin{cases} |\sigma_V| \leqslant \tan(\varepsilon_{V\max}) \\ |\sigma_L| = \tan(\varepsilon_{L\max}) \end{cases} \tag{17}$$

where $\varepsilon_{V\max} \leqslant \pi/2$, $\varepsilon_{L\max} \leqslant \pi/2$.

(iii) Acceleration constraint:

$$\left(\frac{N_V(v_V^{(k)})^2 \sin\varepsilon_V^{(k)}}{r^{(k)}}\right)^2 + \left(\frac{N_L(v_L^{(k)})^2 \sin\varepsilon_L^{(k)}}{r^{(k)}}\right)^2 \leqslant a_{\max}^2. \tag{18}$$

(iv) Terminal constraints:

$$\begin{cases} r(r_f) = r_f^* \\ \lambda_V(r_f) = \theta_V^* \\ \sigma_V(r_f) = 0 \\ \lambda_L(r_f) = \theta_L^* \\ \sigma_L(r_f) = 0 \end{cases}. \tag{19}$$

To satisfy all these constraints, the objective function is transformed into a discrete form:

$$J = -\int_{r_0}^{r_f} \left(\frac{(v_V^{(k)})^3 \sigma_V^{(k)} \sin\varepsilon_V^{(k)} (N_V^{(k)})^2}{r^2} + \frac{(v_L^{(k)})^3 \sigma_L^{(k)} \sin\varepsilon_L^{(k)} (N_L^{(k)})^2}{r^2} \right) \mathrm{d}r. \tag{20}$$

Thus, the optimal control problem can be expressed as follows:

$$\text{Problem A: minimize (20)}$$
$$\text{subject to (13), (16)} - \text{(19)}.$$

3.3 Discretization

The linearized dynamic equation (13) has been discretized to realize convexity. The independent variable r is divided into N segments $\{r_0, r_1, r_2, \ldots, r_N\}$, and the ith discretized point is obtained by $r_i = r_0 + i\Delta r$ $(i = 1, 2, \ldots, N)$, where $\Delta r = (r_f - r_0)/N$. The state vector $\boldsymbol{x}$ and the control vector $\boldsymbol{u}$ are given by $\boldsymbol{x}_i = \boldsymbol{x}(r_i)$ and $\boldsymbol{u}_i = \boldsymbol{u}(r_i)$. The state equation can be numerically integrated by the Euler rule:

$$\boldsymbol{x}_i = \boldsymbol{x}_{i-1} + \Delta r(\boldsymbol{A}_{i-1}^k \boldsymbol{x}_{i-1} + \boldsymbol{B}_{i-1}^k \boldsymbol{u}_{i-1} + \boldsymbol{b}_{i-1}^k) \tag{21}$$

where $\boldsymbol{A}_i^k = \boldsymbol{A}(\boldsymbol{x}^k(r_i))$, $\boldsymbol{B}_i^k = \boldsymbol{B}(\boldsymbol{x}^k(r_i))$ and $\boldsymbol{b}_i^k = \boldsymbol{b}(\boldsymbol{x}^k(r_i))$. By rearranging and combining the same terms, (21) can be rewritten as follows:

$$\boldsymbol{H}_{i-1}\boldsymbol{x}_{i-1} - \boldsymbol{H}_i\boldsymbol{x}_i + \boldsymbol{G}_{i-1}\boldsymbol{u}_{i-1} = -\Delta r\boldsymbol{b}_{i-1}^k \tag{22}$$

where $\boldsymbol{H}_{i-1} = \boldsymbol{I} + \Delta r\boldsymbol{A}_{i-1}^k$, $\boldsymbol{H}_i = \boldsymbol{I}$, $\boldsymbol{G}_{i-1} = \Delta r\boldsymbol{B}_{i-1}^k$, and $\boldsymbol{I}$ is the identity matrix with the same dimensions as $\boldsymbol{A}_i^k$.

Let a new vector be $\boldsymbol{z}=(\boldsymbol{x}_0,\boldsymbol{x}_1,\ldots,\boldsymbol{x}_N,\boldsymbol{u}_0,\boldsymbol{u}_1,\ldots,\boldsymbol{u}_N)^{\mathrm{T}}$; thus, the linearized dynamic equation (13) is transformed into an equality constraint:

$$\boldsymbol{M}\boldsymbol{z}=\boldsymbol{F} \tag{23}$$

where

$$\boldsymbol{M}=\begin{pmatrix} \boldsymbol{I} & \boldsymbol{0} & \boldsymbol{0} & \cdots & \boldsymbol{0} & \boldsymbol{0} & \boldsymbol{0} & \boldsymbol{0} & \cdots & \boldsymbol{0} & \boldsymbol{0} \\ \boldsymbol{H}_0 & \boldsymbol{H}_1 & \boldsymbol{0} & \cdots & \boldsymbol{0} & \boldsymbol{0} & \boldsymbol{G}_0 & \boldsymbol{0} & \cdots & \boldsymbol{0} & \boldsymbol{0} \\ \vdots & \vdots & \vdots & \ddots & \vdots & \vdots & \vdots & \vdots & \ddots & \vdots & \vdots \\ \boldsymbol{0} & \boldsymbol{0} & \boldsymbol{0} & \cdots & \boldsymbol{H}_{N-1} & \boldsymbol{H}_N & \boldsymbol{0} & \boldsymbol{0} & \cdots & \boldsymbol{G}_{N-1} & \boldsymbol{0} \end{pmatrix}$$

and $\boldsymbol{F}=-\Delta r\begin{pmatrix} -\dfrac{1}{\Delta r}\boldsymbol{x}_0 \\ \boldsymbol{x}_0^k \\ \vdots \\ \boldsymbol{x}_{N-1}^k \end{pmatrix}$.

After linearization, convexity and discretization, all constraints and the performance index are transformed into a linear or SOCP problem. As long as the discrete step is small enough, the optimization Problem O is sufficiently close to Problem A:

$$\begin{aligned}&\text{Problem O: minimize (20)}\\ &\qquad\text{subject to (23), (16)} - \text{(19)}.\end{aligned}$$

4. Convex problem solution

The successive steps for solving Problem O are designed as follows.

Step 1 Let $k=0$. Initialize state vector $\boldsymbol{x}^{(0)}$ and control vector $\boldsymbol{u}^{(0)}$ according to the scenario. Vectors $\boldsymbol{x}^{(0)}$ and $\boldsymbol{u}^{(0)}$ do not have to satisfy the look angle constraint and the acceleration constraint because they are used only to generate initial values of $\boldsymbol{A}(\boldsymbol{x}^{(0)})$, $\boldsymbol{B}(\boldsymbol{x}^{(0)})$ and $\boldsymbol{c}(\boldsymbol{x}^{(0)})$.

Step 2 In the $(k+1)$th iteration, SOCP Problem O is established by vectors $\{\boldsymbol{x}^{(k)},\boldsymbol{u}^{(k)}\}$. Then, Problem O is solved to obtain the solution $\{\boldsymbol{x}^{(k+1)},\boldsymbol{u}^{(k+1)}\}$.

Step 3 Check whether the tight convergence constraint is met:

$$\max_i|\boldsymbol{x}_i^{(k+1)}(r)-\boldsymbol{x}_i^{(k)}(r)|\leqslant\boldsymbol{\xi}. \tag{24}$$

Equation (24) consists of a series of component-wise inequalities, and $\boldsymbol{\xi}\in\mathbf{R}^4$ is a constant vector different from the trust-region constraint. If this constraint is satisfied, then proceed to Step 4; otherwise, let $k=k+1$ and return to Step 2.

Step 4 The iteration needs to be stopped. A converged solution $\{\boldsymbol{x}^{(k+1)},\boldsymbol{u}^{(k+1)}\}$ is obtained.

The control energy is minimized by the above steps. The conventional PN guidance law cannot satisfy the acceleration constraint, whereas the convex optimal method can deal with multiconstraint problems. If the control vector $\boldsymbol{u}_{i+1}$ cannot be obtained in the $(i+1)$th discretized point, it is set to be replaced by $\boldsymbol{u}_i$ to ensure the stability and reliability of guidance.

5. Numerical examples

A ground-to-ground scenario is designed to demonstrate the validity of the solution proposed in this paper. Suppose a missile has a constant velocity of 200 m/s and a range to go of 4 000 m. The constraints are set as: $\varepsilon_{V\max}=50^\circ$, $\varepsilon_{L\max}=50^\circ$ and $a_{\max}=50$ m/s^2. The trust-region constraint is set as:

$$\boldsymbol{\delta}=\begin{pmatrix}60\pi/180 & \tan(60\pi/180) & 60\pi/180 & \tan(60\pi/180)\end{pmatrix}^{\mathrm{T}}. \tag{25}$$

The convergence constraint is set as follows:

$$\boldsymbol{\xi}=\begin{pmatrix}2\pi/180 & \tan(2\pi/180) & 2\pi/180 & \tan(2\pi/180)\end{pmatrix}^{\mathrm{T}}. \tag{26}$$

The optimization problem is modeled by the software MOSEK [32]. Simulations are performed on a computer configured with CPUi7-4790@3.6 GHz and 8 GB of memory.

5.1 Two-dimensional guidance

First, two-dimensional simulation is performed to verify the effectiveness of the method in this paper. Compared with the traditional two-dimensional model, the model here is still the three-dimensional model, although the initial and terminal states in plane MLT are set as zero. θ_f^* is designed as the expected terminal flight path angle. r_{tgo} is designed as the range to go. The initial and terminal parameters are stated in Table 1.

Table 1 Two-dimensional flight parameters

Parameter	Initial value/(°)	Terminal value/(°)
LOS angle in MVT	0	−60, −90, −120
LOS angle in MLT	0	0
Flight path angle in MVT	15	−60, −90, −120
Flight path angle in MLT	0	0
Look angle in MVT	15	0
Look angle in MLT	0	0

Because a missile attacks a target with different impact angles, the angular relations in Fig. 5 of those terminal flight path angle constraints with respect to one another satisfy the look angle constraint and the initial and terminal

conditions. The results show that different terminal LOS angle constraints greatly affect the guidance gain profiles and the corresponding acceleration profiles. The smaller the expected terminal LOS angle, the higher the absolute values of the initial guidance gain and the acceleration. A higher altitude of the trajectory corresponds to a smaller expected terminal LOS angle. When the impact angle is given, the proposed method converges in approximately 3.2 s to obtain the solution to Problem O.

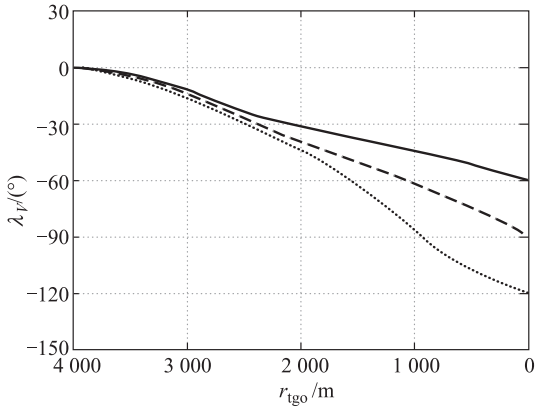

(a) LOS angle

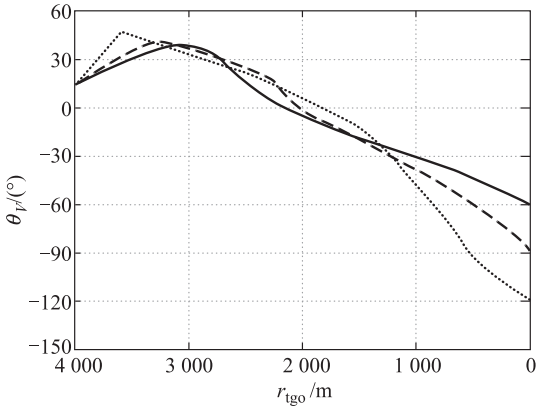

(b) Flight path angle

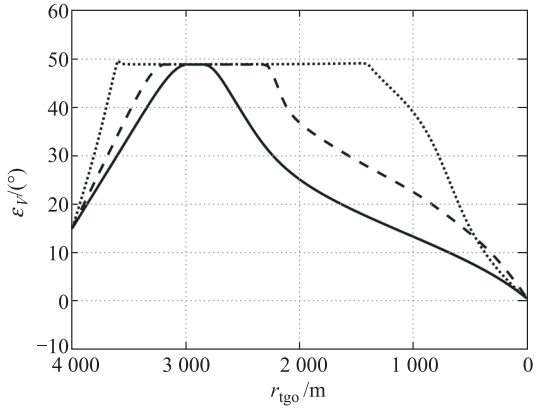

(c) Look angle

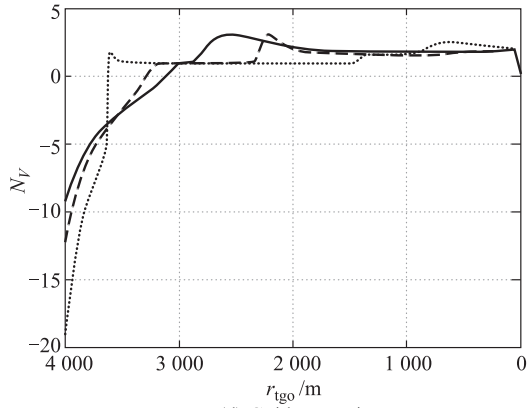

(d) Guidance gain

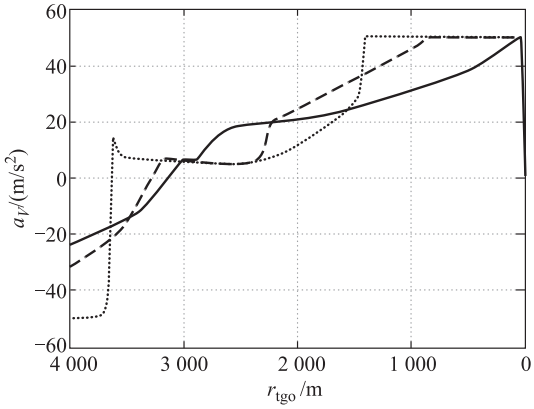

(e) Acceleration

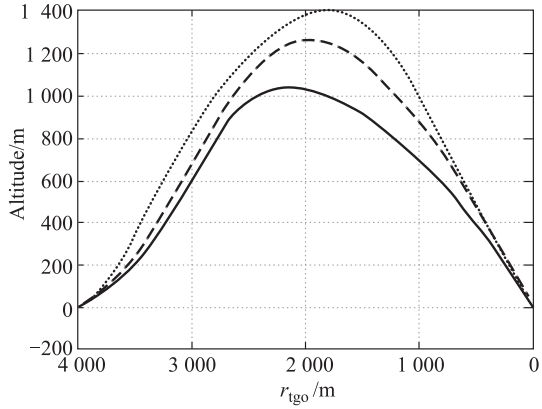

(f) Altitude

——: $\theta_f^*=-60°$; – – –: $\theta_f^*=-90°$; ·····: $\theta_f^*=-120°$.

Fig. 5 Two-dimensional profiles with different impact angles in *MVT*

Angles, acceleration and lateral displacement in plane MLT remain at approximately zero during the flight in Fig. 6. Empirically, the values $N_V \leqslant 20$ and $N_L \leqslant 20$ are implemented to avoid divergence and the guidance gain N_L is maximized in the range from 500 m to 3 000 m. The reason for this phenomenon is detailed in the next section for the same condition under three-dimensional guidance.

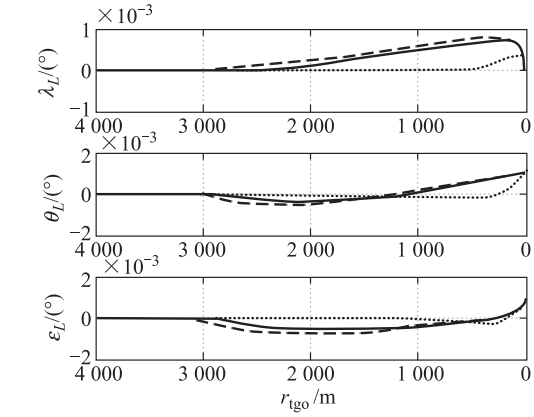

(a) Angle parameters

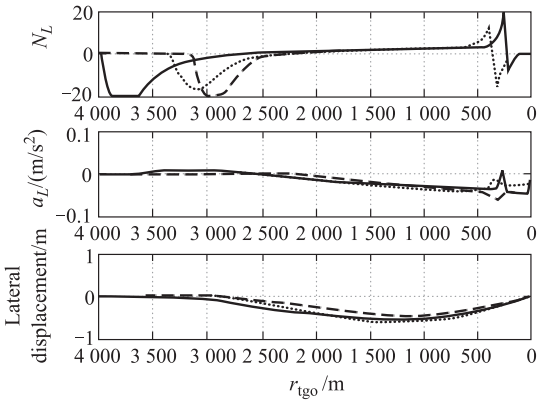

(b) Control parameters

——: $\theta_f^*=-60°$; – – –: $\theta_f^*=-90°$; ·····: $\theta_f^*=-120°$.

Fig. 6 Two-dimensional profiles with different impact angles in MLT

5.2 Three-dimensional guidance with a constant velocity

Three-dimensional simulations are performed in this section. The initial or terminal parameters in planes MVT and MLT are designed to be the same as those in Table 2.

Table 2 Three-dimensional flight parameters

Parameter	Initial value/(°)	Terminal value/(°)
LOS angle in MVT	0	−60, −90, −120
LOS angle in MLT	0	0
Flight path angle in MVT	15	−60, −90, −120
Flight path angle in MLT	15	0
Look angle in MVT	15	0
Look angle in MLT	15	0

All constraints can be satisfied for both plane MVT and plane MLT in Fig. 7. Parameters in plane MLT change significantly because the initial flight path angle and the look angle in plane MLT are set to 15°, which is a different value from that of the two-dimensional simulation. When the impact angle is given, the proposed method converges in approximately 3.2 s to obtain the solution to Problem O.

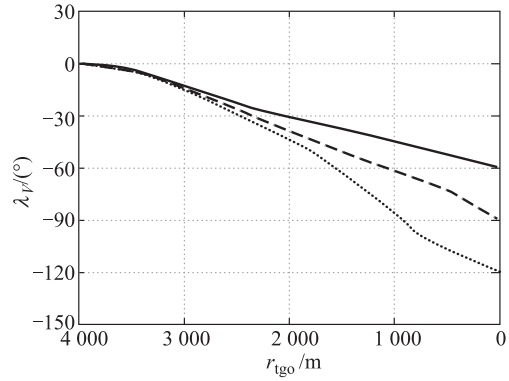

(a) LOS angle in MVT

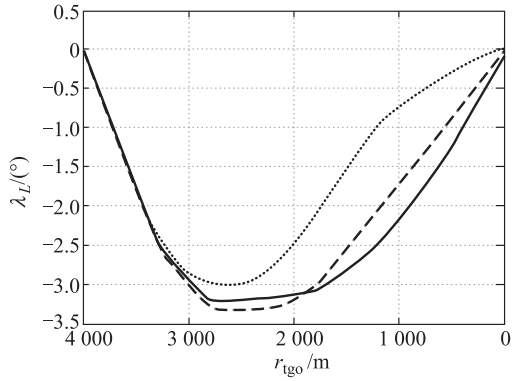

(b) LOS angle in MLT

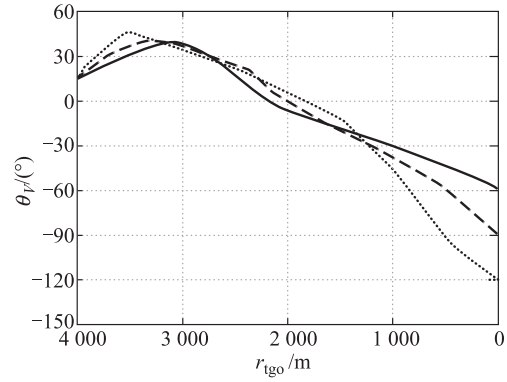

(c) Flight path angle in MVT

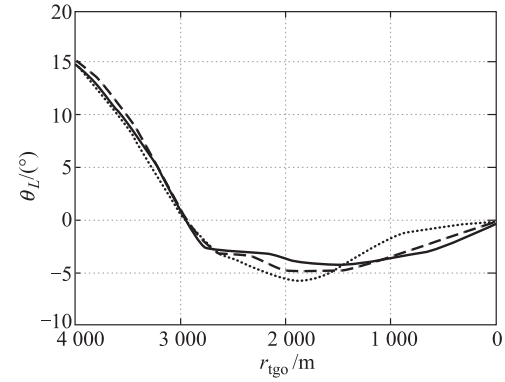

(d) Flight path angle in MLT

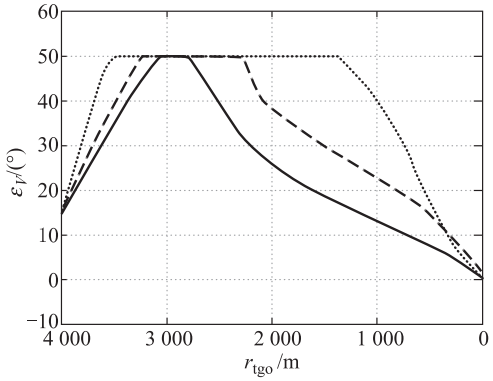

(e) Look angle in MVT

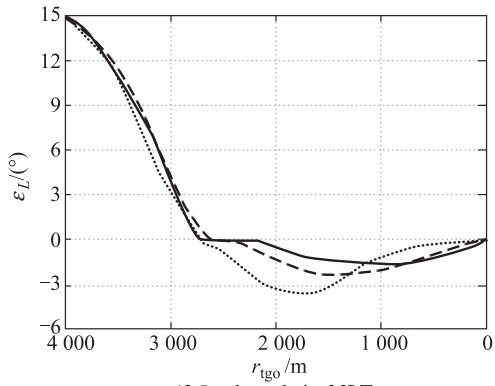

(f) Look angle in MLT

: $\theta_f^*=-60°$; : $\theta_f^*=-90°$; : $\theta_f^*=-120°$.

Fig. 7 Three-dimensional angle profiles with a constant velocity

The guidance gain N_L reaches the maximum near 2 500 m, which is similar to the two-dimensional simulation. We find that the look angle in the MLT plane is close to 0 in Fig. 7. Thus, the performance index for plane MLT in the objective function becomes out of control. The most likely outcome is a divergent control vector. Therefore, empirically limiting the guidance law is necessary. The terminal flight path angle constraints for plane MVT affect the parameters of plane MLT in Fig. 8 according to the three-dimensional engagement kinematics in (1) and (2).

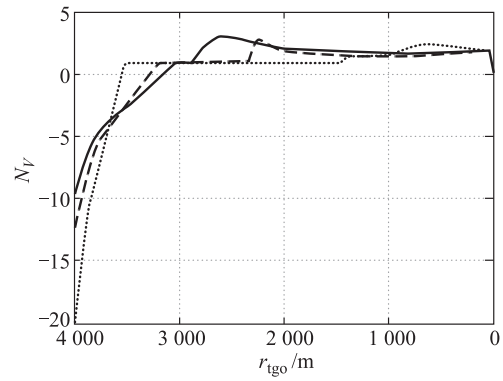

(a) Guidance gain in MVT

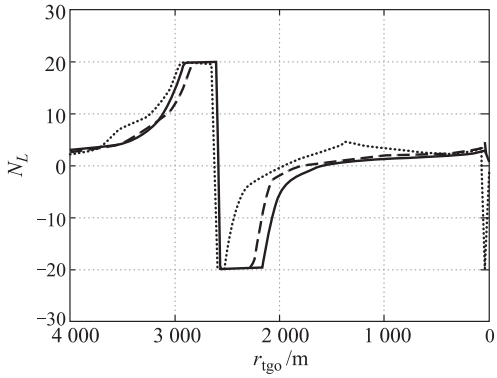

(b) Guidance gain in MLT

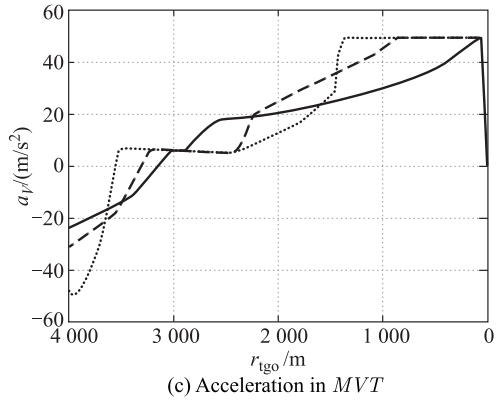

(c) Acceleration in MVT

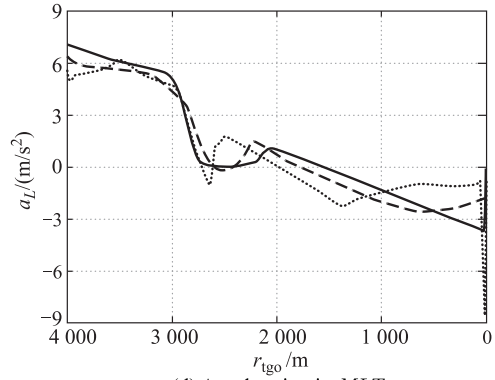

(d) Acceleration in MLT

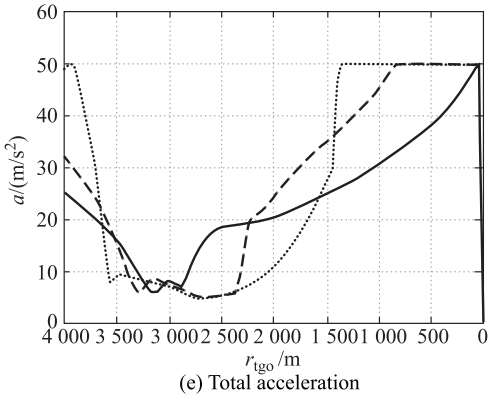

(e) Total acceleration

: $\theta_f^*=-60°$; : $\theta_f^*=-90°$; : $\theta_f^*=-120°$.

Fig. 8 Three-dimensional guidance profiles with a constant velocity

Thus, a guidance law ignoring mutual coupling between planes is feasible. Fig. 8 shows that all constraints are satisfied during the flight.

Profiles for the altitude and lateral displacement with different impact angles and a more indicative view of the trajectory in three dimensions are shown in Fig. 9.

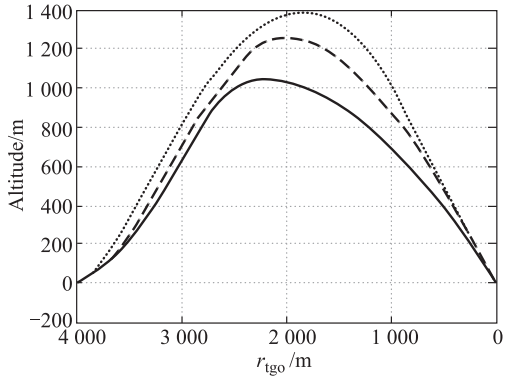

(a) Altitude in MVT

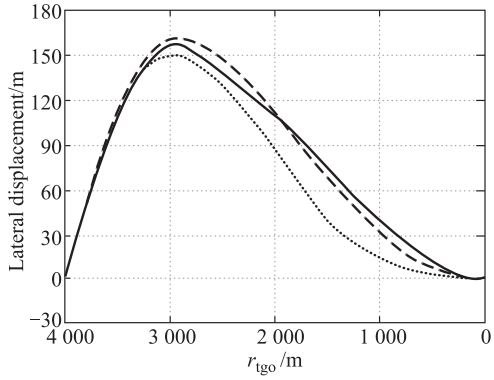

(b) Lateral displacement in MLT

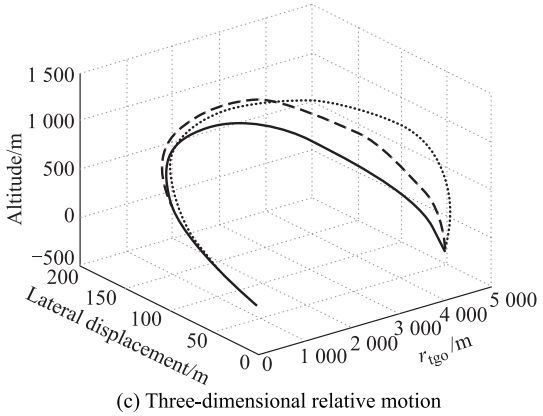

(c) Three-dimensional relative motion

——: $\theta_f^*=-60°$; – – – –: $\theta_f^*=-90°$; ·····: $\theta_f^*=-120°$.

Fig. 9 Three-dimensional position profiles with a constant velocity

5.3 Three-dimensional guidance with a time-varying velocity

For a missile with a time-varying velocity, the velocity can be approximated by the last guidance circle. The increment of the velocity is given by the following:

$$\Delta V = -\frac{D}{m} - g\sin\theta_V \tag{27}$$

where $D = 0.5\rho V^2 S_{ref} C_D$ is the aerodynamic drag, m is the mass, and g is the gravitational acceleration. We set $\rho = 1.225\text{e}^{-0.001h(0.108-0.4\times10^{-5}h)}$, $S_{ref} = 0.1$ m^2, $C_D = 0.02$, $m = 40$ kg, and $g = 9.81$ m/s^2, where h is the altitude. The velocity V used to calculate the aerodynamic drag is obtained by the last guidance circle, and the velocity in the new guidance circle is given by $V + \Delta V$.

Other conditions are the same as those in Section 5.2. All constraints of the terminal angles can be satisfied for both plane MVT and plane MLT in Fig. 10.

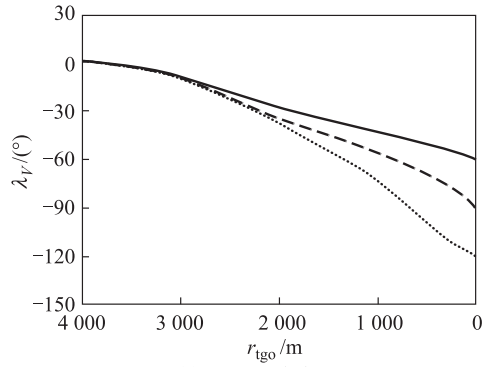

(a) LOS angle in MVT

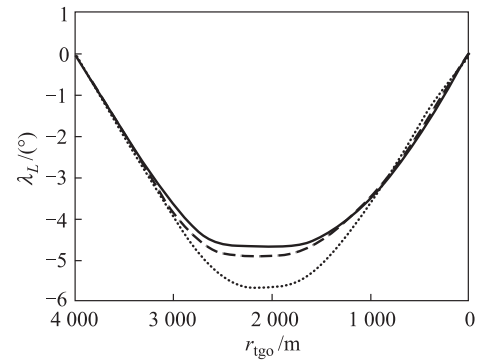

(b) LOS angle in MLT

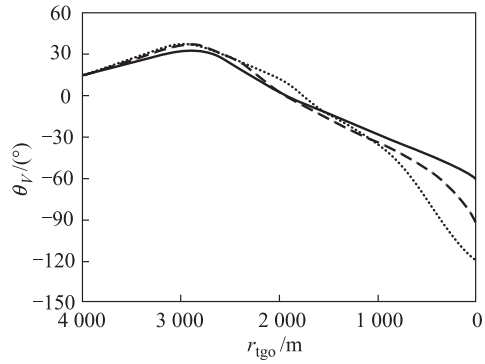

(c) Flight path angle in MVT

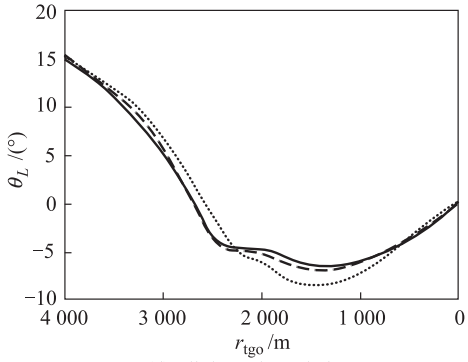

(d) Flight path angle in MLT

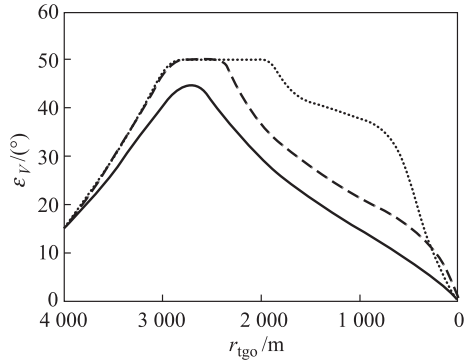

(e) Look angle in MVT

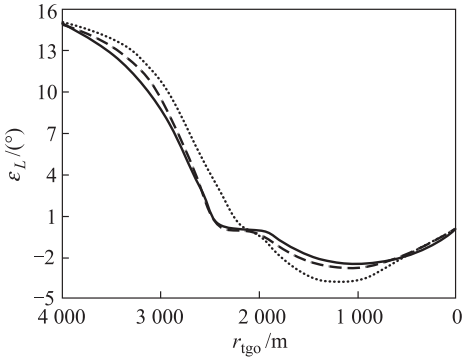

(f) Look angle in MLT

——— : $\theta_f^*=-60°$; — — — : $\theta_f^*=-90°$; ····· : $\theta_f^*=-120°$.

Fig. 10 Three-dimensional angle profiles with a time-varying velocity

When the impact angle is given, the proposed method converges in approximately 3.2 s to obtain the solution to Problem O.

For a missile with a time-varying velocity, the guidance gain and acceleration in plane MVT in Fig. 11 are significantly different from those of a missile with a constant velocity in Fig. 8. The guidance gain and acceleration decrease, especially in the initial phase. The total acceleration satisfies the constraint, and the velocity profiles are very close for different impact angles.

Profiles for the altitude and lateral displacement with different impact angles and a more indicative view of the trajectory in three dimensions with a time-varying velocity are shown in Fig. 12.

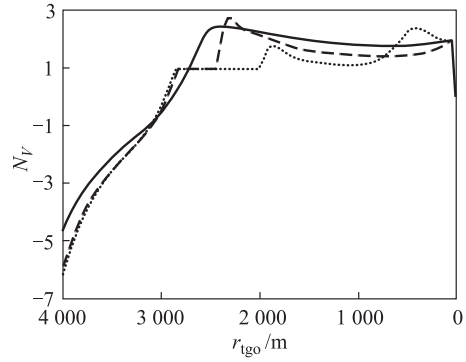

(a) Guidance gain in MVT

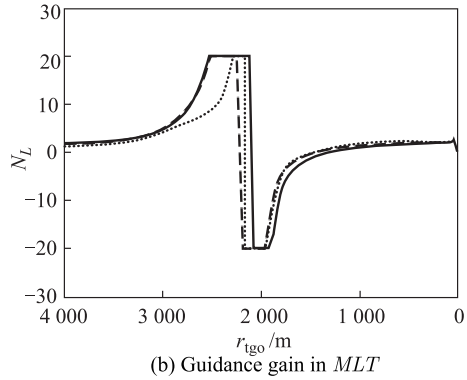

(b) Guidance gain in MLT

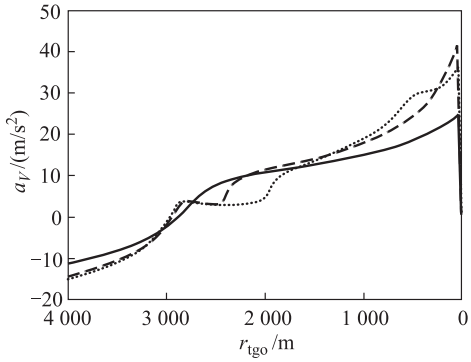

(c) Acceleration in MVT

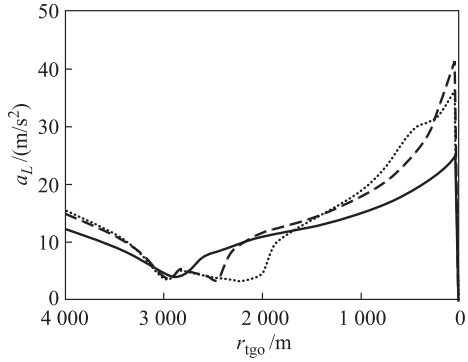

(d) Acceleration in MLT

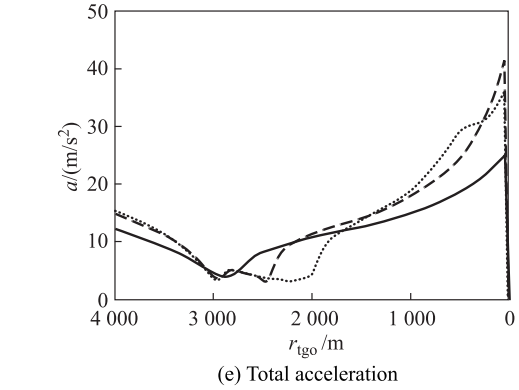

(e) Total acceleration

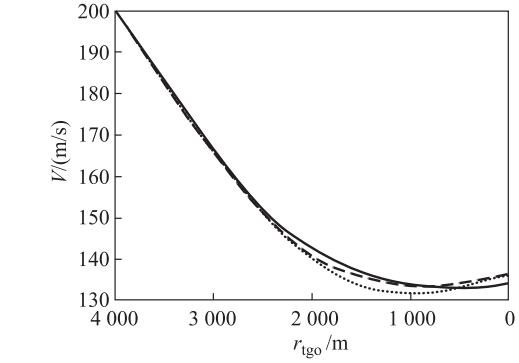

(f) Velocity

——: $\theta_f^*=-60°$; – – – –: $\theta_f^*=-90°$; ·····: $\theta_f^*=-120°$.

Fig. 11 Three-dimensional guidance profiles with a time-varying velocity

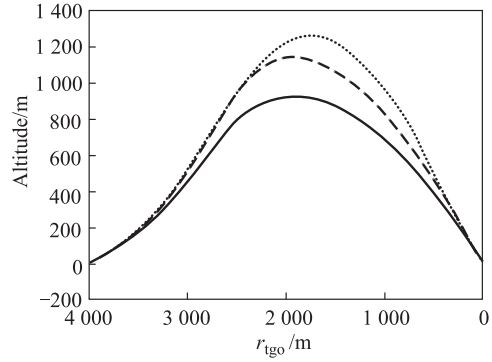

(a) Altitude in MVT

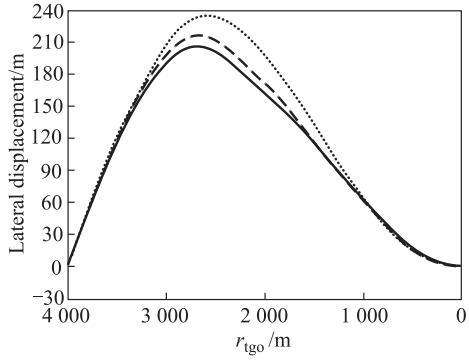

(b) Lateral displacement in MLT

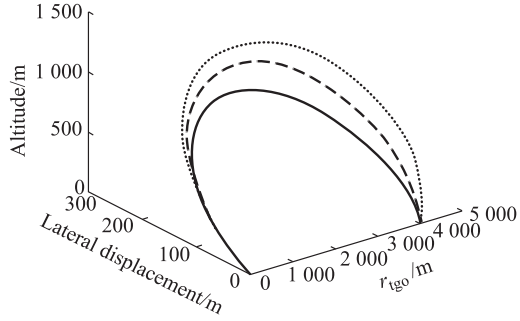

(c) Three-dimensional relative motion

——: $\theta_f^*=-60°$; – – – –: $\theta_f^*=-90°$; ·····: $\theta_f^*=-120°$.

Fig. 12 Three-dimensional position profiles with a time-varying velocity

6. Conclusions

In this paper, a reliable and adaptive three-dimensional guidance law subject to common initial, look angle, acceleration, and terminal constraints is developed by using convex optimization. For three-dimensional engagement kinematics with PN, the three-dimensional space is divided into two planes and the coupling between planes is ignored. The simplified model can transform the second-order constraint into an SOCP problem for convexity. Through linearization, convexity and discretization, all constraints and the performance index are transformed into a linear or SOCP problem, and the convex optimal control problem can be obtained by the continuous solution method. The simulation results show that the adaptive three-dimensional guidance law is suitable for two-dimensional and three-dimensional engagement kinematics with a constant or a time-varying velocity. This method can satisfy all the constraints, and it could possibly be applied for online guidance in future research.

Compared with the traditional guidance law, the requirement of the acceleration constraint can be realized using the proposed method. However, the method has some shortcomings in terms of accuracy. Future studies could try to find a more accurate solution to three-dimensional modeling.

References

[1] ACIKMESE B, PLOEN S R. Convex programming approach to powered descent guidance for Mars landing. Journal of Guidance, Control, and Dynamics, 2007, 30(5): 1353 – 1366.

[2] BLACKMORE L, ACIKMESE B, SCHARF D P. Minimum-landing-error powered-descent guidance for Mars landing using convex optimization. Journal of Guidance, Control, and Dynamics, 2010, 33(4): 1161 – 1171.

[3] ACIKMESE B, CARSON J M, BLACKMORE L. Lossless convexification of nonconvex control bound and pointing constraints of the soft landing optimal control problem. IEEE

Trans. on Control Systems Technology, 2013, 21(6): 2104 – 2113.
[4] HARRIS M W, BEHÇET A. Maximum divert for planetary landing using convex optimization. Journal of Optimization Theory and Applications, 2014, 162(3): 975 – 995.
[5] YANG H, BAI X L, BAOYIN H X. Rapid generation of time-optimal trajectories for asteroid landing via convex optimization. Journal of Guidance, Control, and Dynamics, 2017, 40(3): 628 – 641.
[6] LIU X F, LU P. Solving nonconvex optimal control problems by convex optimization. Journal of Guidance, Control, and Dynamics, 2014, 37(3): 750 – 765.
[7] CHAKRABORTY N, PENG J, AKELLA S, et al. Proximity queries between convex objects: an interior point approach for implicit surfaces. IEEE Trans. on Robotics, 2008, 24(1): 211 – 220.
[8] LIN P, REN W, WANG H, et al. Multiagent rendezvous with shortest distance to convex regions with empty intersection: algorithms and experiments. IEEE Trans. on Cybernetics, 2018, 49(3): 1026 – 1034.
[9] LEIZAROWITZ A. Existence of overtaking optimal trajectories for problems with convex integrands. Mathematics of Operations Research, 1985, 10(3): 450 – 461.
[10] WANG Z B, GRANT M J. Autonomous entry guidance for hypersonic vehicles by convex optimization. Journal of Spacecraft and Rockets, 2018, 55(4): 993 – 1005.
[11] ZHAO D J, SONG Z Y. Reentry trajectory optimization with waypoint and no-fly zone constraints using multiphase convex programming. Acta Astronautica, 2017, 137: 60 – 69.
[12] LIU X F, SHEN Z J, LU P. Entry trajectory optimization by second-order cone programming. Journal of Guidance, Control, and Dynamics, 2016, 39(2): 227 – 241.
[13] LOBO M S, VANDENBERGHE L, BOYD S, et al. Applications of second-order cone programming. Linear Algebra and its Applications, 1998, 284(1/2/3): 193 – 228.
[14] ALIZADEH F, XIA Y. The Q method for second-order cone programming. Computers Operations Research, 2008, 35(5): 1510 – 1538
[15] ANDERSEN E D, ROOS C, TERLAKY T. On implementing a primal-dual interior-point method for conic quadratic optimization. Mathematical Programming, 2003, 95(2): 249 – 277.
[16] MURTAUGH S A, CRIEL H E. Fundamentals of proportional navigation. IEEE Spectrum, 1966, 3(12): 75 – 85.
[17] GUELMAN M. A qualitative study of proportional navigation. IEEE Trans. on Aerospace and Electronic Systems, 1971, AES-7(4): 637 – 643.
[18] SHIN H S, LEE J I, TSOURDOS A. A new homing guidance law to reduce sensitivity on initial heading errors. Proceedings of the Institution of Mechanical Engineers, Part G: Journal of Aerospace Engineering, 2015, 229(9): 1740 – 1753.
[19] KIM M, GRIDER K V. Terminal guidance for impact attitude angle constrained flight trajectories. IEEE Trans. on Aerospace and Electronic Systems, 1973, 9(6): 852 – 859.
[20] HO Y, BRYSON A, BARON S. Differential games and optimal pursuit-evasion strategies. IEEE Trans. on Control Systems Technology, 1965, 10(4): 385 – 389.
[21] ERER K S, OSMAN M. Indirect impact-angle-control against stationary targets using biased pure proportional navigation. Journal of Guidance, Control, and Dynamics, 2012, 35(2): 700 – 704.
[22] SONG J M, ZHANG T Q. Passive homing missile's variable structure proportional navigation with terminal angular constraint. Chinese Journal of Aeronautics, 2001, 14(2): 83 – 87.
[23] ZHANG Y X, SUN M, CHEN Z. Finite-time convergent guidance law with impact angle constraint based on sliding-mode control. Nonlinear Dynamic, 2012, 70(1): 619 – 625.
[24] WU P, YANG M. Integrated guidance and control design for missile with terminal impact angle constraint based on sliding mode control. Journal of Systems Engineering and Electronics, 2010, 21(4): 623 – 628.
[25] SHASHI R K, DEBASISH G. Sliding mode guidance for impact time and angle constraints. Proceedings of the Institution of Mechanical Engineers, Part G: Journal of Aerospace Engineering, 2018, 232 (16): 2961 – 2977.
[26] PARK B G, KIM T H, TAHK M J. Range-to-go weighted optimal guidance with impact angle constraint and seeker's look angle limits. IEEE Trans. on Aerospace and Electronic Systems, 2016, 52(3): 1241 – 1256.
[27] TEKIN R, ERER K S. Switched-gain guidance for impact angle control under physical constraints. Journal of Guidance, Control, and Dynamics, 2015, 38(2): 205 – 216.
[28] JEON I S, LEE J I. Impact-time-control guidance law with constraints on seeker look angle. IEEE Trans. on Aerospace and Electronic Systems, 2017, 53(5): 2621 – 2627.
[29] KIM T H, PARK B G, TAHK M J. Bias-shaping method for biased proportional navigation with terminal-angle constraint. Journal of Guidance, Control, and Dynamics, 2013, 36(6): 1810 – 1816.
[30] LIU X F, SHEN Z J, LU P. Closed-loop optimization of guidance gain for constrained impact. Journal of Guidance, Control, and Dynamics, 2017, 40(2): 453 – 460.
[31] HUAN J, AN Z, YU Y N, et al. Cooperative guidance with multiple constraints using convex optimization. Aerospace Science and Technology, 2018, 79: 426 – 440.
[32] ANDERSEN E D, ROOS C, TERLAKY T. On implementing primal-dual interior-point method for conic quadratic optimization. Mathematical Programming, 2003, 95(2): 249 – 277.

Biographies

FU Shengnan was born in 1993. She received her B.E. degree from Beijing Institute of Technology in 2014. She is currently a doctoral student in the School of Mechatronical Engineering, Beijing Institute of Technology. Her main research interests include flight vehicle design, guidance and control.
E-mail: 3120160497@bit.edu.cn.com

LIU Xiaodong was born in 1987. He received his Ph.D. degree from School of Automation Science and Electrical Engineering, Beihang University in 2013. Now he is a senior engineer with Beijing Aerospace Automatic Control Institute. His main research interests include flight vehicle design, guidance and control.
E-mail: k.start@163.com

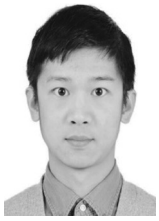

ZHANG Wenjie was born in 1992. He received his B.E. degree from Beijing Institute of Technology in 2015. He is currently a doctoral student at the School of Aerospace Engineering, Beijing Institute of Technology. His main research interests include flight vehicle design, guidance and control.
E-mail: bit_zhangwenjie@outlook.com

XIA Qunli was born in 1971. He received his Ph.D. degree from the School of Aerospace Engineering, Beijing Institute of Technology. Now he is a professor with Beijing Institute of Technology. His research interests are control and guidance technology.
E-mail: 1010@bit.edu.cn